energies

MDPI

Article

Hybrid Modulated Model Predictive Control in a Modular Multilevel Converter for Multi-Terminal Direct Current Systems

Zhi Wu [1], Jiawei Chu [1], Wei Gu [1,*], Qiang Huang [2], Liang Chen [2] and Xiaodong Yuan [2]

[1] School of Electrical Engineering, Southeast University, Nanjing 210096, China; zwu@seu.edu.cn (Z.W.); 220152251@seu.edu.cn (J.C.)
[2] Jiangsu Electrical Power Company Research Institute, State Grid, Nanjing 211100, China; grassstrong@163.com (Q.H.); lancing_chen@163.com (L.C.); lannyyuan@hotmail.com (X.Y.)
* Correspondence: wgu@seu.edu.cn; Tel.: +86-25-8779-6169

Received: 17 May 2018; Accepted: 11 July 2018; Published: 17 July 2018

Abstract: In this paper a hybrid modulated model predictive control (HM^2PC) strategy for modular-multilevel-converter (MMC) multi-terminal direct current (MTDC) systems is proposed for supplying power to passive networks or weak AC systems, with the control objectives of maintaining the DC voltage, voltage stability and power balance of the proposed system. The proposed strategy preserves the desired characteristics of conventional model predictive control method based on finite control set (FCS-MPC) methods, but deals with high switching frequency, circulating current and steady-state error in a superior way by introducing the calculation of the optimal output voltage level in each bridge arm and the specific duty cycle in each Sub-Module (SM), both of which are well-suited for the control of the MMC system. In addition, an improved multi-point DC voltage control strategy based on active power balanced control is proposed for an MMC-MTDC system supplying power to passive networks or weak AC systems, with the control objective of coordinating the power balance between different stations. An MMC-HVDC simulation model including four stations has been established on MATLAB/Simulink (r2014b MathWorks, Natick, MA, USA). Simulations were performed to validate the feasibility of the proposed control strategy under both steady and transient states. The simulation results prove that the strategy can suppress oscillations in the MMC-MTDC system caused by AC side faults, and that the system can continue functioning if any one of the converters are tripped from the MMC-MTDC network.

Keywords: MMC-MTDC; hybrid modulated model predictive control; optimal output voltage level; multi-point DC control

1. Introduction

In recent years, MMCs are gaining a lot of attention in high power/high voltage applications that involve interfacing high-voltage direct current (HVDC) systems to high voltage three-phase AC grids due to their high modularity and scalability [1,2]. Investment and research in high-voltage direct-current (HVDC) systems has been actively pursued and expanded with the aim of improving the efficiency and reliability of electric power generation, large-capacity power transmission, and linkage among different networks [1–6].

At present, research on control strategies for MMC-HVDC systems has yielded fruitful results in industry and academia. When an MMC-HVDC transmission system supplying passive networks is operating normally, its rectifier station generally uses constant current control and constant reactive control, which contains an outer power loop and an inner current loop. This control method is relatively

mature and fixed, and details on the method are available in the literature [6–10]. Therefore, in this paper we focus on the control strategy used in the inverter station.

Traditional inverter station control usually involves a double closed-loop control (DCLC) strategy based on an outer voltage loop and an inner current loop. Since the response speed of the outer voltage loop is significantly slower than that of the inner current loop, the voltage quality is poor when supplying power to nonlinear loads. Furthermore, the response time of the voltage recovery increases when there are load fluctuations. Meanwhile, the overall control structure, embodying multiple proportional-integral (PI) controllers with hard-to-tune parameters, is relatively complex, and is therefore susceptible to structural parameters of the model [11,12].

Model predictive control (MPC) is gradually becoming more adopted as a control method of power converters because it is a non-linear optimization control method that can deal with nonlinear systems with complex constraints. The advantages demonstrated by this method are diverse, such as a fast response, flexibility of various goals, easy inclusion of nonlinearities, and the availability of simple modulation techniques. The MPC method based on a finite control set (FCS-MPC) constructs a multi-objective optimization function, evaluates the system's future state corresponding to the finite-switching combination of the converter, and selects the switch combination that minimizes the value of the objective function as the switching state for the next switching cycle. MPC has been applied to motor drives, high power factor rectification, and DC transmission, among others [13–21].

Reference [13] shows that the cost function may include a control target such as reduced switching frequency, reduced common-mode voltage, reduced reactive power, and reduced current ripple when controlling a power converter. Compared to proportional integral (PI) or proportional-resonant (PR) controllers, the MPC method can improve total harmonic distortion (THD) and transient characteristics [21]. References [16–18] uses FCS-MPC for the control of the MMC, which predicts the AC current, the circulating current, the sub-module capacitance voltage, and the resulting switching action of all possible switch combinations of the upper and lower arms in each control cycle. This method selects the switch combination that minimizes the objective function as the output of the next cycle and implements multi-objective optimal control.

For an MMC system with a large number of sub-modules, the existing FCS-MPC control methods involve a large amount of calculation. The Modulated Model Predictive Control (M^2PC) method preserves all the advantages of the FCS-MPC method and solves some problems associated with the FCS-MPC method, such as enabling variable switching frequency, delay compensation, and short sampling times [22–24]. However, little to no effort has been made to develop a M^2PC method for the control of MMC-HVDC systems supplying power to passive networks or weak AC systems. This paper aims to propose a new Hybrid M^2PC method for control of the MMC-MTDC system that addresses the key limitations faced by the FCS-MPC methods.

The contributions of this paper to the research field are:

(1) A novel voltage control strategy based on M^2PC is proposed for MMC-MTDC systems supplying power to passive networks or weak AC systems, which effectively regulates AC line currents and allows converters to comply with current references under severe conditions, such as severe power fluctuations or grid faults.

(2) The proposed strategy reduces the amount of calculation required compared with FCS-MPC methods when calculating optimal output voltage levels.

(3) An improved multi-point DC voltage control strategy based on active power balanced control is proposed and proved to be more applicable to MMC-MTDC systems.

2. MMC-MTDC Mathematical Model

Figure 1 shows the schematic diagram of a four-terminal MMC-MTDC system for supplying passive networks.

The rectifiers and inverters are made of three-phase MMCs. In the figure, L_s and L_p represent the AC filter inductances, while R_s and R_p denote the line equivalent resistances. U_{s1} and U_{s2} represent two

independent AC power supplies. u_s and u_p represent the AC voltage of the sending end of the rectifier station and the receiving end of the inverter station, respectively. i_{dc} represents the current of the DC line. Further, C_{dc} denotes the DC capacitor, and C_1 and L_1 (C_3 and L_3) constitute the LC low-pass filter, which filters out the high-order harmonics on the inverter side, while C_2 can also provide some of the AC network reactive power support to compensate for the impact of load fluctuations on voltage stability.

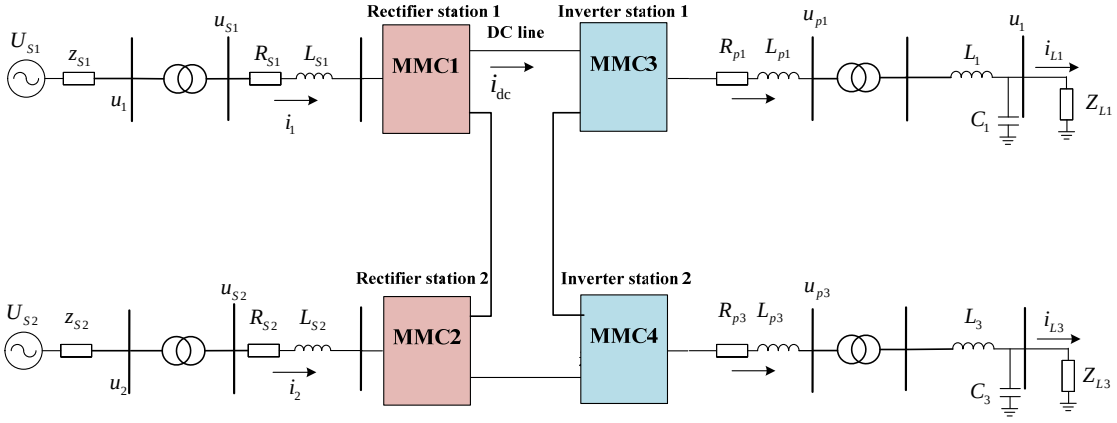

Figure 1. System configuration of a modular multilevel converter based multi-terminal direct current (MMC-MTDC) system for supplying passive networks.

Figure 2a presents the Circuit diagram of the inverter side of a three-phase MMC with six arms. Generally speaking, each arm is composed of a half-bridge submodule (SM). The MMC legs consist of three phases, a, b, and c, which are represented by the subscript j. Subscripts u and l represent the upper and lower arms of each leg. N series-connected SM, as well as the equivalent internal resistance (R) and an inductor (L), make up each leg. R_{p1} and L_{p1} denote the AC filter inductance and the line equivalent resistance of inverter station 1. Figure 2b shows the circuit diagram of SM. The switches T1 and T2 always operate in a complementary fashion.

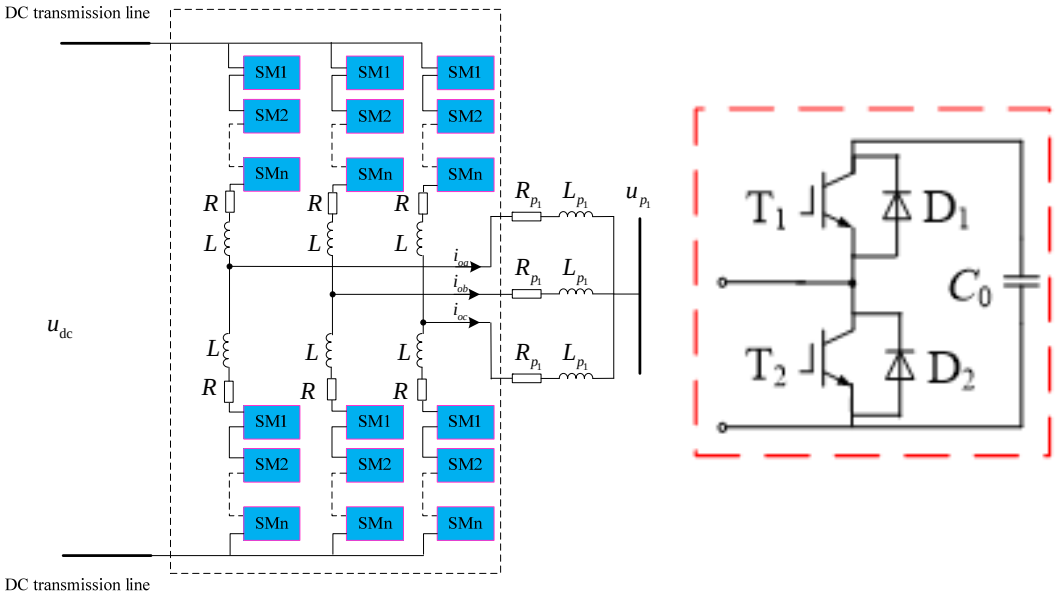

(**a**) (**b**)

Figure 2. Circuit diagram of MMC: (**a**) Circuit diagram of the inverter side of a three-phase MMC; (**b**) Circuit diagram of Sub-Module (SM).

Using Kirchhoff's Voltage Law (KVL), the transient mathematical model of the AC side of an MMC can be obtained,

$$\frac{\mathrm{d}i_{sj}}{\mathrm{d}t} = \frac{1}{L_{se}}(2u_{dj} - 2u_{p_1 j} - R_{se}i_{sj}) \tag{1}$$

$$\frac{\mathrm{d}i_{cj}}{\mathrm{d}t} = \frac{1}{L}(u_{dc} - u_{cj} - Ri_{cj}) \tag{2}$$

where

$$\begin{cases} u_{cj} = \frac{1}{2}(u_{uj} + u_{lj}) \\ u_{dj} = -\frac{1}{2}(u_{uj} - u_{lj}) = \frac{1}{2}(u_{lj} - u_{uj}) \\ i_{cj} = \frac{1}{2}(i_{uj} + i_{lj}) \end{cases} \quad \text{and} \quad \begin{cases} L_{se} = L + 2L_{p_1} \\ R_{se} = R + 2R_{p_1} \end{cases}$$

where u_{cj} and u_{dj} denote common voltage and differential voltage, respectively, and i_{cj} represents circulation current.

Under balanced control the capacitor voltages of each sub module are equal, and the output voltage of the upper and lower bridge arm varies from 0 and N levels:

$$\begin{cases} u_{uj} = \frac{n_{uj}}{N} u_{\mathrm{dc}},\ n_{uj} \in [0, 1, \cdots, N] \\ u_{lj} = \frac{n_{lj}}{N} u_{\mathrm{dc}},\ n_{uj} \in [0, 1, \cdots, N] \end{cases} \tag{3}$$

where n_{uj} and n_{lj} represent the number of SMs for upper and lower arm inputs, respectively, and u_{uj} and u_{lj} represent the voltages of the upper and lower arms, respectively.

3. Design of the Hybrid Modulated Model Predictive Control Strategy

3.1. Design of the Inverter Side Controller

$$\Psi_{sj}(t) = \frac{1}{L_{se}}(2u_{dj} - 2u_{p_1 j} - R_{se}i_{sj}) \tag{4}$$

$$\Psi_{cj}(t) = \frac{1}{L}(u_{dc} - u_{cj} - Ri_{cj}) \tag{5}$$

Let T_s represent the sampling time, kT_s represent the present moment and $(k+1)T_s$ represent the moment at the next control period. Utilizing the trapezoidal integration formula in Equation (4),

$$i_{sj}(k+1) - i_{sj}(k) = \frac{T_s}{2}(\Psi_{sj}(k+1) + \Psi_{sj}(k)) \tag{6}$$

Considering that the fluctuation of u_{sj} is negligible over one sampling period from kT_s to $(k+1)T_s$, it can be approximated as invariant. Thus, the discretization of Equation (4) can be obtained,

$$i_{sj}(k+1) = \frac{2L_{se} - T_s\, R_{se}}{2L_{se} + T_s\, R_{se}} i_{sj}(k) + \frac{4T_s}{2L_{se} + T_s\, R_{se}} u_{dj}(k) - \frac{2T_s}{2L_{se} + T_s\, R_{se}}(u_{p_1 j}(k+1) + u_{p_1 j}(k)) \tag{7}$$

Similarly, considering that u_{dc} is constant during the sampling time, Equation (4) can be rewritten as,

$$i_{cj}(k+1) = i_{cj}(k) + \frac{T_s}{L}(u_{dc}(k) - u_{cj}(k)) \tag{8}$$

Equations (6) and (8) can be used to predict the AC line and circulating current values for all combinations of SM operations.

M^{2}PC requires a suitable modulation scheme as part of the minimization of the cost function in the MPC algorithm. In this paper we use a modulation scheme that is particularly suitable for high power converter control. In each sampling period, only one branch of one SM is allowed to switch, so as to obtain the total switching frequency of the SM, which is half of the sampling frequency [22–24].

This function becomes quite important when considering high power applications. Moreover, this switching mode helps to reduce the computational needs of the controller.

The proposed M^{2}PC method evaluates a cost function $J(k)$ for all possible voltage levels in each leg at the start of each sampling period. This cost function with multiple prediction horizons can be defined as,

$$J_{p_1 j}(k+1) = \left| u_{p_1 j}(k+1) - u^*_{p_1} \right| \tag{9}$$

where

$$u^*_{p_1 j} = U^*_s e^{j2\pi f^*(k+1)T_s} \tag{10}$$

where U_s* represents the rated AC voltage; f* = 50 Hz is the rated frequency [25].

By combining Equations (1)–(3) and (6), the reference voltage level of the bridge arm satisfying the AC voltage and the current control target is obtained,

$$\begin{cases} n^*_{uj} = \frac{N}{2u_{\mathrm{dc}}}(u^*_{sj}(k+1) + u^*_{cj}(k+1)) \\ n^*_{lj} = \frac{N}{2u_{\mathrm{dc}}}(u^*_{cj}(k+1) - u^*_{sj}(k+1)) \end{cases} \tag{11}$$

where n_{uj}* and n_{lj}* represent the reference voltage levels of n_{uj} and n_{lj}, respectively.

In general, the number of sub-modules applied to the MMC is large. If the traditional FCS-MPC control strategy is used, the computational load is undoubtedly enormous [26]. This paper uses Equation (11) to calculate the optimal output level of the bridge arm at the next sampling time, and then considers its neighboring $2M$ ($M \geq 1$) levels as a finite control set by selecting the appropriate M value, which can significantly reduce the amount of calculations in one control cycle. It is worth noting that in most cases n_{uj}* and n_{lj}*, calculated according to Equation (11), are not integers. This paper uses the method of rounding down, then selects the level combination and the upper or lower bridges. The $2M$ level combinations adjacent to the arm together constitute a new set of modulable finite controls.

A key point of voltage control in the M^{2}PC strategy proposed in this paper is to calculate n_{uj} and n_{lj} based on the two specific voltage values of the passive network output voltage and the circulating current suppression voltage, based on Equation (11) [27–29]. The reference value thus minimizes the state performance function in Equation (7) based on the non-monotonic change characteristic of $J_{zj}(k+1)$. From the structural characteristics of the MMC it can be seen that, whether it is the upper or lower arms, increasing the number of levels in the bridge arm can increase the output value of the control target to the passive network at a future point, while reducing the number of arm levels will reduce the output voltage value to the passive network.

Therefore, the corresponding upper and lower arm level configuration parameters can be calculated according to the voltage prediction reference value at the beginning of the next period. Let the increase and decrease in the number of levels of the j phase affect the output voltage values of the next period by $V_j{}^1$ and $V_j{}^2$, respectively. In one control period described by setting a specific time node $t_{p_1 j}$ executing the control commands one after another leads $u_{p_1 j}$ $(k+1)$ to finally equal $u^*_{p_1 j}$.

The ratio of time changing between $V_j{}^1$ and $V_j{}^2$ is called the duty cycle. The details of calculating this duty cycle for the proposed M^{2}PC method are explained in detail in Reference [30]. Employing the formulation from Reference [30], the duty cycle can be obtained as,

$$d_{p_1 j} = \frac{u^*_{p_1 j} - u^2_{p_1 j}}{u^1_{p_1 j} - u^2_{p_1 j}} \tag{12}$$

where $u^1_{p_1 j}$ and $u^2_{p_1 j}$ can be obtained from Equation (10) by substituting $u_{sj}(k)$ with $V_j{}^1$ and $V_j{}^2$ respectively. In Equation (12), $d_{p_1 j}$ represents the time ratio of $u_{sj}(k)$ needs to be set to $V_j{}^1$.

Similarly, the cost function and the duty cycle corresponding to the circulating current are,

$$J_{cj}(k+1) = \left| i_{cj}(k+1) - i^*_{cj} \right| \tag{13}$$

$$d_{cj} = \frac{i_{cj}^{*} - i_{cj}^{2}}{i_{cj}^{1} - i_{cj}^{2}} \tag{14}$$

3.2. Improvement of the Model Predictive Control Algorithm

The performance cost function of Equation (13) guarantees an optimal combination of converter switches in one control cycle, but does not take into account its optimality in two or more control cycles, ignoring suboptimal switch combinations or other combinations which contain the optimal information. The algorithm relies on strong assumptions about the load behavior, and non-linear loads and load fluctuations may cause converter control system oscillation and even divergence. This paper will improve the algorithm with multi-step output predictive control to improve its robustness.

Firstly, single step prediction is performed using the discrete state equation. The number of inserted submodules (SM) is then determined to meet the requirements of multi-step model prediction. Figures 3 and 4 illustrate the principle of one step M^{2}PC and the proposed optimized multi-step M^{2}PC, respectively. One of the most distinctive feature of the proposed optimized multi-step M^{2}PC is that its predicted periods become multi-step, and its control periods remain one step. Taking two-step in Figure 4 as an example, there are many paths that allow $u_{P_1 j}$ to reach the reference value at $(k+2)T_s$, but only one path minimizes the cost function, which could be more optimized than the path in Figure 3.

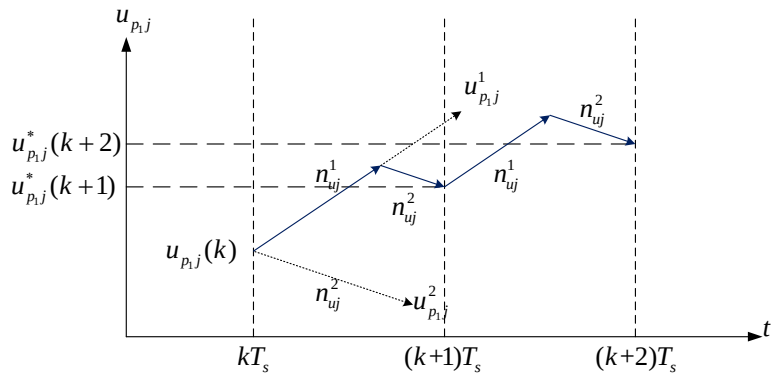

Figure 3. Principle of one step Modulated Model Predictive Control (M^{2}PC).

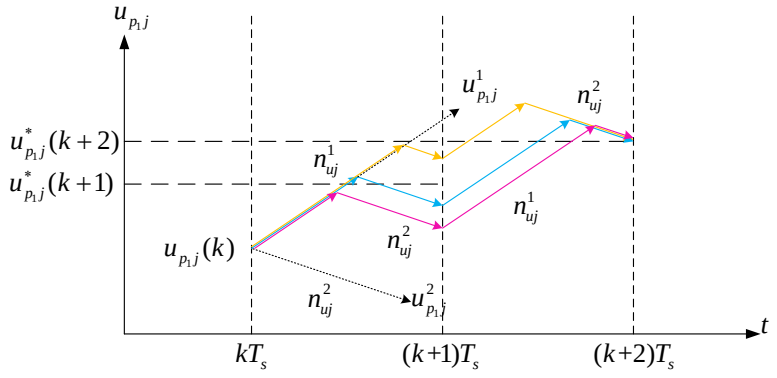

Figure 4. Principle of proposed optimized multi-step M^{2}PC.

Therefore, the key principle of the proposed strategy is to solve for the optimal solution of the predictive model in multiple periods. In this situation, the value of the state variable in the multi-step predictive model ($X(k+p)$) needs to be calculated, and the cost function needs to make corresponding adjustments. Taking the two-step situation as an example, this paper utilizes Simpson's formula

to calculate $X(k+2)$, which can minimize the calculation error. For multi-step cases, Runge-Kutta formulae can be used.

Taking two-step in Figure 4 as an example, utilizing the Simpson integration formula in Equations (4) and (5),

$$i_{sj}(k+2) - i_{sj}(k) = \frac{T_s}{6}(\Psi_{sj}(k+2) + 4\Psi_{sj}(k+1) + \Psi_{sj}(k)) \tag{15}$$

$$i_{cj}(k+2) - i_{cj}(k) = \frac{T_s}{6}(\Psi_{cj}(k+2) + 4\Psi_{cj}(k+1) + \Psi_{cj}(k)) \tag{16}$$

Similarly, considering that u_{sj} and u_{dc} are constant during the sampling time,

$$J(k+1) = \lambda_1 \left| u_{p_1 j}(k+2) - u^*_{p_1} \right| + \lambda_2 \left| i_{cj}(k+2) - i^*_{cj} \right| \tag{17}$$

where λ_1 to λ_2 are the weighting factors of each control target.

Considering the computational complexity of the performance cost function at this time, as well as taking into account the robustness of the multi-step prediction, M can be set to 1. Meanwhile, for simplicity, it can be assumed that the load current does not change within the predicted time domain. Thus, the improved VSC-HVDC system inversion and the corresponding performance cost function are constructed using the improved Equations (15) and (16).

When a DC fault occurs, it should be noted that the fluctuation of the terminal voltage will be comparatively greater. This will undoubtedly result in instability of the controlled output voltage of the converter and the limit of the voltage range to be reached.

The DC voltage reference value of the DC voltage control link in the original converter station control system is corrected according to the amount of voltage fluctuation, and the threshold value of the modified voltage reference signal is applied to ensure that the DC voltage of the multi terminal system will not deviate from the normal operating range.

3.3. Total Cost Function and Duty Cycles

The cost function is now given by,

$$J(k+1) = \lambda_1 J_{pj}(k+2) + \lambda_2 J_{cj}(k+2) \tag{18}$$

The two weighting factors, λ_1 and λ_2 can be adjusted to achieve the desired the control performance. Since the current cost function $J_{cj}(k+2)$ already includes the amount of current necessary to charge the DC-link capacitor to the desired voltage, the importance of $J_{pj}(k+2)$ lies in its ability to reduce the steady-state error in the DC-link voltage, related to the converter losses, which is not considered in $J_{cj}(k+2)$. Therefore, the ratio λ_1/λ_2 is typically set to the minimum value that ensures zero steady-state error in the DC-link voltage [31,32].

The switching times for the two selected vectors are calculated by solving the linear system of equations in Equation (18). Once the value of K is obtained from Equation (18), the expressions for the switching times are obtained

$$\begin{cases} J_{cj}^{(1)} = \frac{K}{J_{cj}^{(1)}} \\ d_{cj}^{(2)} = \frac{K}{J_{cj}^{(2)}} \\ d_{cj}^{(1)} + d_{cj}^{(2)} = 1 \end{cases} \Rightarrow \begin{cases} d_{cj}^{(1)} = \frac{J_{cj}^{(2)}}{J_{cj}^{(1)} + J_{cj}^{(2)}} \\ d_{cj}^{(2)} = \frac{J_{cj}^{(1)}}{J_{cj}^{(1)} + J_{cj}^{(2)}} \end{cases} \tag{19}$$

Once the switching times are calculated, the M^{2}PC algorithm chooses the two inverter states for times $d_{cj}^{(1)}$ and $d_{cj}^{(2)}$ if they minimize the following global cost function:

$$J_{cj} = d_{cj}^{(1)} G_{cj}^{(1)} + d_{cj}^{(2)} G_{cj}^{(2)} \tag{20}$$

This solution is proposed as an alternative to an analytical duty cycle calculation. The overall M^{2}PC scheme is shown in Figure 5.

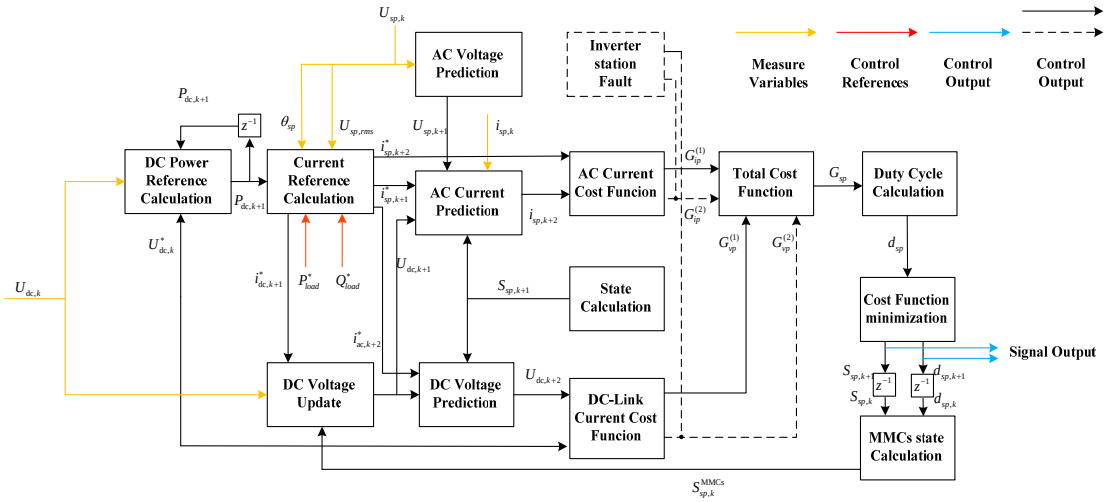

Figure 5. Overall M^{2}PC block scheme for the control of MMC converters.

3.4. Improved Multi-Point DC Voltage Control Strategy

The proposed multi-step M^{2}PC control strategy is mainly used on the inverter stations connected to the loads as a first control, while the multi-point voltage coordinated control strategy is used between these four stations to maintain the balance of active power and the stability of DC voltage as a secondary control.

Therefore, this paper further proposes a multi-point voltage coordinated control strategy based on M^{2}PC and power balance, which is called Hybrid M^{2}PC (HM^{2}PC). HM^{2}PC is integrated into the primary and secondary coordination control strategy, and its specifics are as follows:

(1) MTDC multi-point voltage coordination control requires the upper system-level controller to provide the active power reference signal to the converter station-level controller of each terminal converter station.

(2) In the upper system level controller, either the converter station with the largest converter capacity or the key converter station in the system is selected as the power balance converter station. The reference values for the active power of the remaining converter stations are taken directly from the power flow regulator system, while the reference values for the active power of the converter stations are calculated according to Equation (21), based on the reference values for the active powers of other converter stations. The variable n is the number of MTDC converter stations.

$$P_{Balance} = -\sum (P_{ref1}, P_{ref2}, \cdots\cdots, P_{refn-1}) \tag{21}$$

(3) The system level control system only updates the active power reference value to each converter station when changing the scheduling trend. At the other times, the converter stations are independently controlled according to the reference value calculated from the active power after the latest update, without much communication needs.

3.5. Implementation of the HM^{2}PC Strategy

The execution of HM^{2}PC includes the following steps:

(1) Sample and measure the relevant electrical parameters of the MMC-HVDC system at time kT_s, including: $u_{pj}(k), u_{sj}(k), u_{dc}(k)$, and $i_{sj}(k)$.

(2) With the prediction model, improved multi-step prediction function, and prediction correction function, combined with the time sampling value kT_s and the inverter switching state for different calculations, calculate the predicted value at the $(k+1)T_s$ moment (or $(k+p)T_s$ moment, $p = 1, 2$).

(3) According to step (2) and the corresponding performance cost function, the predicted output of the traversing method is calculated as the inverter output in the prediction horizon from all possible combinations of the switch performance cost function and the corresponding values.

(4) The performance cost function values corresponding to each switch state are compared, and the minimum switching state g_{min} (i.e., the optimal switching state) is selected to generate switching signals, which are then driven and amplified to act on the inverter.

(5) Repeat step (1) to step (4) at the next sampling period.

4. Simulation Results and Analysis

In order to verify the effectiveness of the above predictive control algorithm, a simulation model of the VSC-MTDC system (Figure 1) in MATLAB/Simulink has been developed. The system parameters are listed in Table 1. In this study, the constant current control and constant reactive control strategy are adopted on the rectifier side of the VSC-MTDC system. On the inverter side, the traditional DCLC strategy, single-step predictive control strategy, and improved multi-step predictive control strategy (the number of predicted steps P is 3), which is added to the correction feedback, are simulated and compared.

Table 1. Parameters for the Study System of Figure 1 (Sub-Module (SM)).

Quantity	Value
AC sources system nominal Voltage	35 kV
Nominal DC voltage	±10 kV
R_s	0.1 Ω
L_s	5 mH
R_p	0.02 Ω
L_2	1.3 mH
C_2	200 μF
DC capacitance C_{dc}	4700 μF
DC line length	10 km
AC load system nominal voltage	20 kV
The number of stations	4
Arm inductance L	1 mH
Arm resistance R	0.2 Ω
SM capacitor C	1.2 mF
The number of SMs	10

4.1. MMC Converters Connected to the Load

In this simulation scenario the MMC1 stations maintain a voltage of 20 kV and the MMC3 stations maintain a power of 30 kW. Initially, the MMC4 station maintained a constant load of 40 MW. At 5 s, the load was reduced by 16 MW, and the load at 10 s increased by 16 MW, with the MMC3 station adjusting the amount of added power fluctuation.

In order to compare the static characteristics using a nonlinear load between the traditional control strategy and the adaptive modulated model predictive control strategy mentioned in this paper, several large frequency converters are connected to the low-voltage side of the passive network. The control frequency is 10 kHz and the corresponding AC current simulation results are shown in Figure 6.

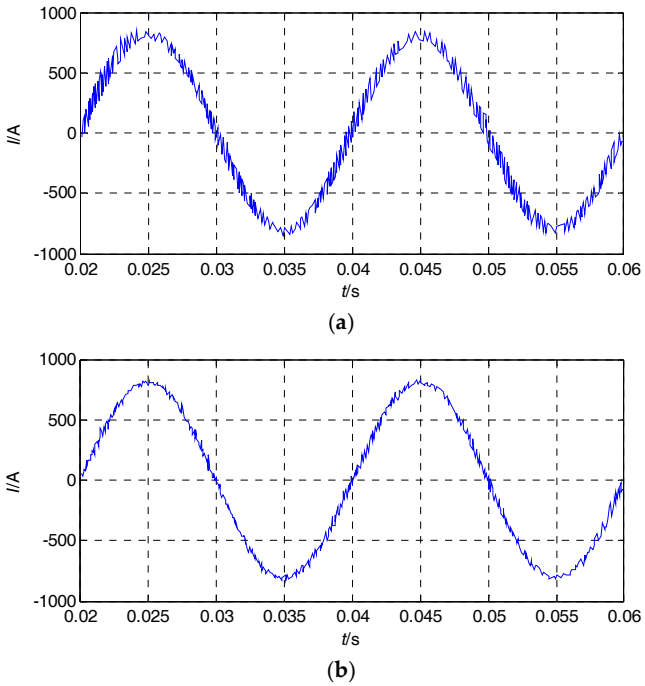

Figure 6. The simulation results of AC current: (**a**) Traditional control strategy; (**b**) The strategy proposed in this paper.

By comparing and calculating the current error of the traditional control strategy and the strategy proposed in this paper, the current signal Total Harmonic Distortion (THD) values are 9.88% and 1.83%, respectively. It can be seen that when large-capacity nonlinear loads are connected to the grid system the quality of the power supply using the traditional control strategy is significantly reduced, while the proposed method can still maintain acceptable static performance. Therefore, in the face of large-scale renewable energy integration into the distribution network, the proposed control strategy has great advantages in ensuring the quality of the power supply.

The simulation results in Figure 7a,b compare the inhibition of circulation current in a MMC converter using M^2PC with the improved multi-step M^2PC. At 0.25 s, the circulation suppression function is enabled separately. As can be seen, the circulation current contains some DC and low harmonic components. After the function is enabled, the circulation current under both control methods is rapidly reduced. The difference is that the improved multi-step M^2PC is able to further reduce the size of the circulation current and lower the amplitude of the pulse in the circulation current.

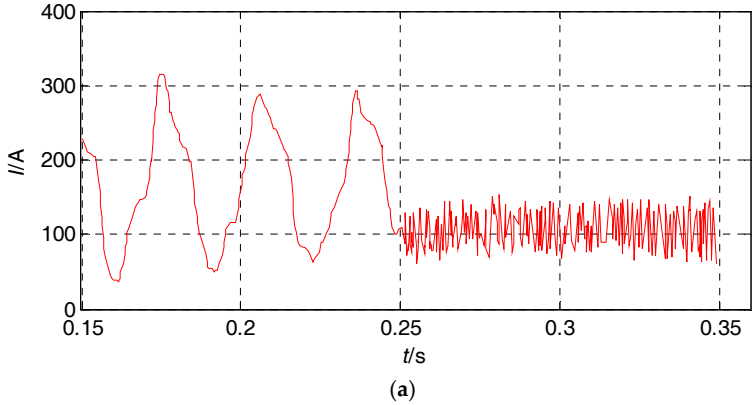

Figure 7. *Cont.*

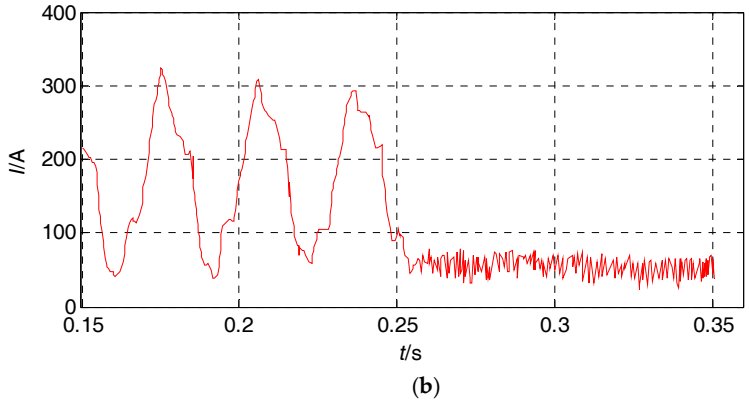

Figure 7. The simulation results of circulation current: (**a**) M^{2}PC; (**b**) Improved multi-step M^{2}PC.

4.2. Regulation Station Supplemental Power During Load Fluctuation

In this simulation scenario, the MMC1 stations maintain their voltage at 20 kV and the MMC3 stations maintain their power at 30 kW. Initially the MMC4 station maintained a constant load of 40 MW. At 5 s, the load was reduced by 16 MW, the load at 10 seconds increased by 16 MW, and the MMC3 station adjusted the amount of added power fluctuation.

The comparison of the active power transmitted by the MMC2 station and the MMC4 station in each coordinated control mode is shown in Figure 8, and the comparison of the DC voltage at each end of the MTDC system is shown in Figure 9.

In this simulation, FCS-MPC is faster than the other two control strategies. However, as the ability to adjust the load fluctuation depends entirely on the master station, the controller should balance the active power and the voltage control a ring DC grid. Furthermore, deficiencies in single point voltage control cause large voltage fluctuations, with the maximum fluctuation threshold reached 5 times. Thus, voltage and power fluctuations as well as the steady state error are the largest of the three kinds of control.

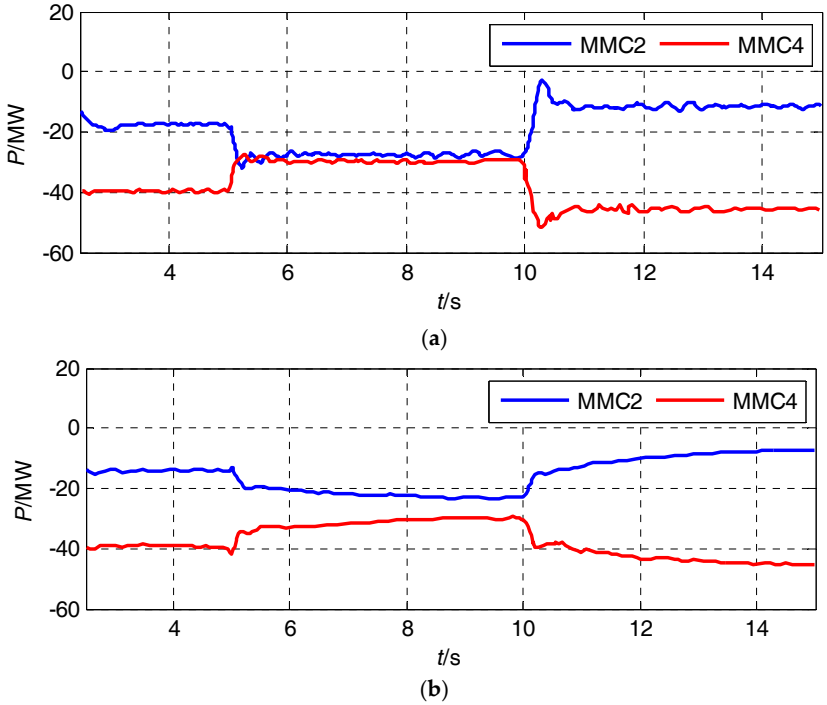

Figure 8. *Cont.*

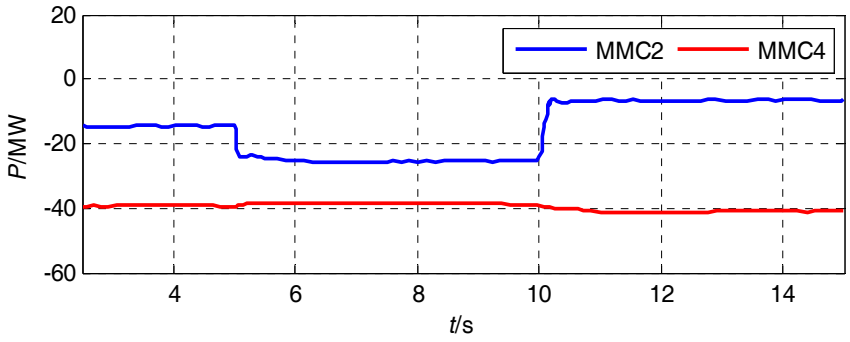

(**c**)

Figure 8. Simulation waveforms of load fluctuation: (**a**) The active power of the receiving end controlled by double closed-loop control (DCLC); (**b**) The active power of receiving end controlled by an MPC method based on a finite control set (FCS-MPC); (**c**) The active power of the receiving end controlled by the hybrid modulated model predictive control (HM^{2}PC).

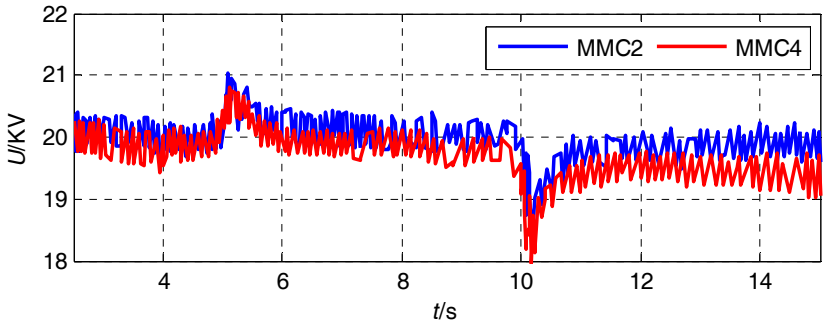

(**a**)

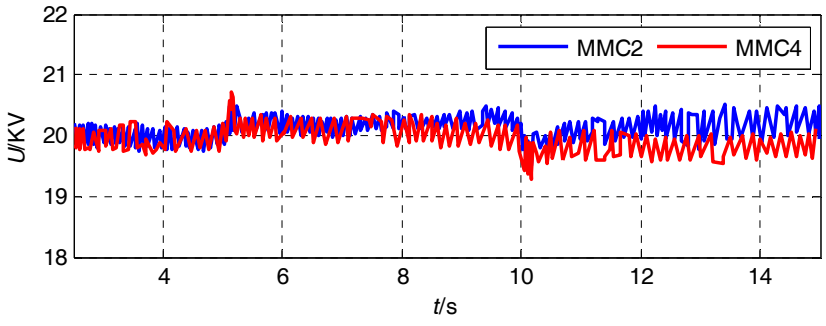

(**b**)

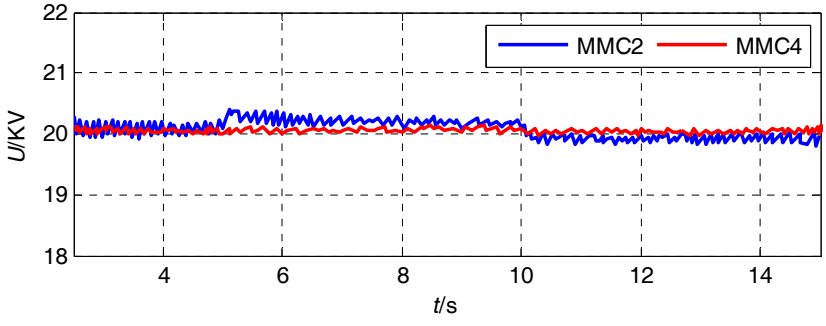

(**c**)

Figure 9. Simulation waveforms of load fluctuation: (**a**) The DC voltage controlled by DCLC; (**b**) the DC voltage controlled by FCS-MPC; (**c**) the DC voltage controlled by the HM^{2}PC.

The HM^{2}PC strategy proposed in this paper is faster than DCLC FCS-MPC. The DC voltage under control shows almost no fluctuation under load fluctuation, and the voltage fluctuation and power fluctuation in steady state are the smallest among the three control modes.

4.3. Aimulating the Exit of the Main Control Station Due to Failure

In this simulation scenario, the MMC1 station and the MMC4 station maintain a constant load of 10 MW and 40 MW, respectively. Initially, the VSC1 station and the VSC3 station respectively issue 20 MW and 30 MW of active power. At 5 s, the main control station MMC1 exited due to a failure. At this time, the MMC3 station became the new main control station and simultaneously delivered power to the MMC2 station and the MMC4 station.

The comparison of the active power transmitted by the MMC2 station and the MMC4 station in each coordinated control mode is shown in Figure 10, and the comparison of the DC voltage at each end of the MTDC system is shown in Figure 11.

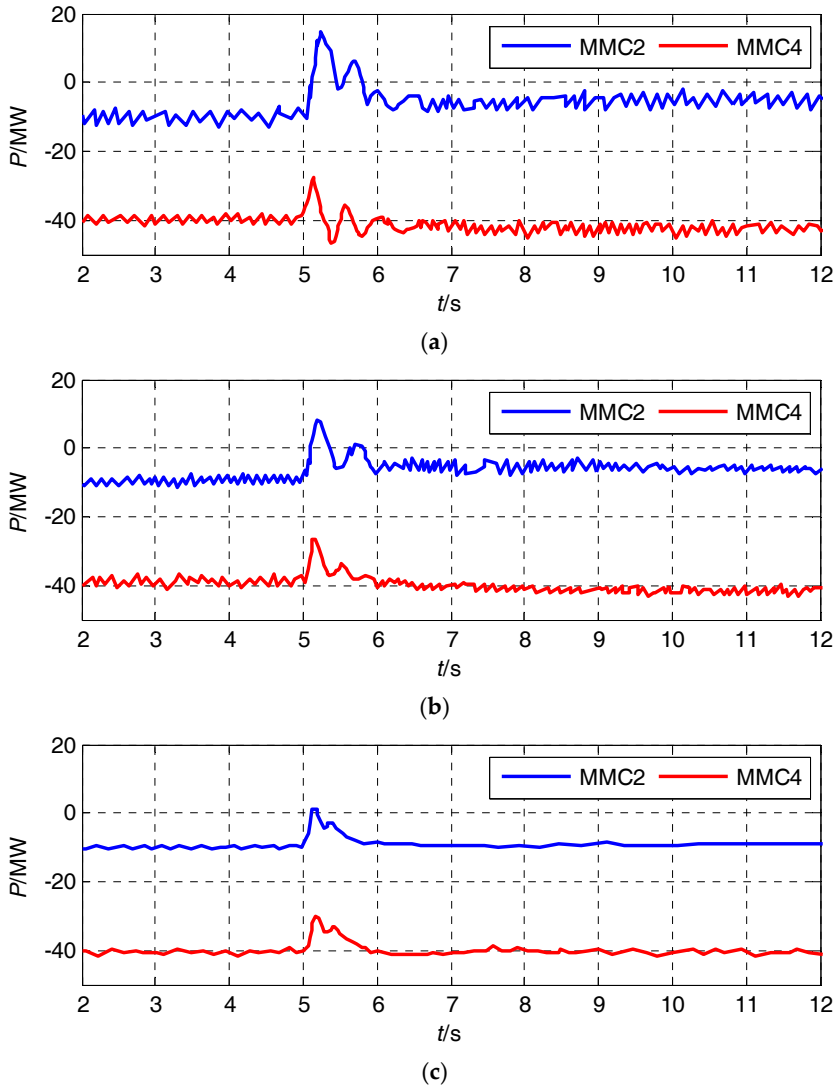

Figure 10. Simulation of the operation during an exit of an input converter station: (**a**) The active power of the receiving end controlled by DCLC; (**b**) the active power of the receiving end controlled by FCS-MPC; (**c**) the active power of the receiving end controlled by HM^{2}PC.

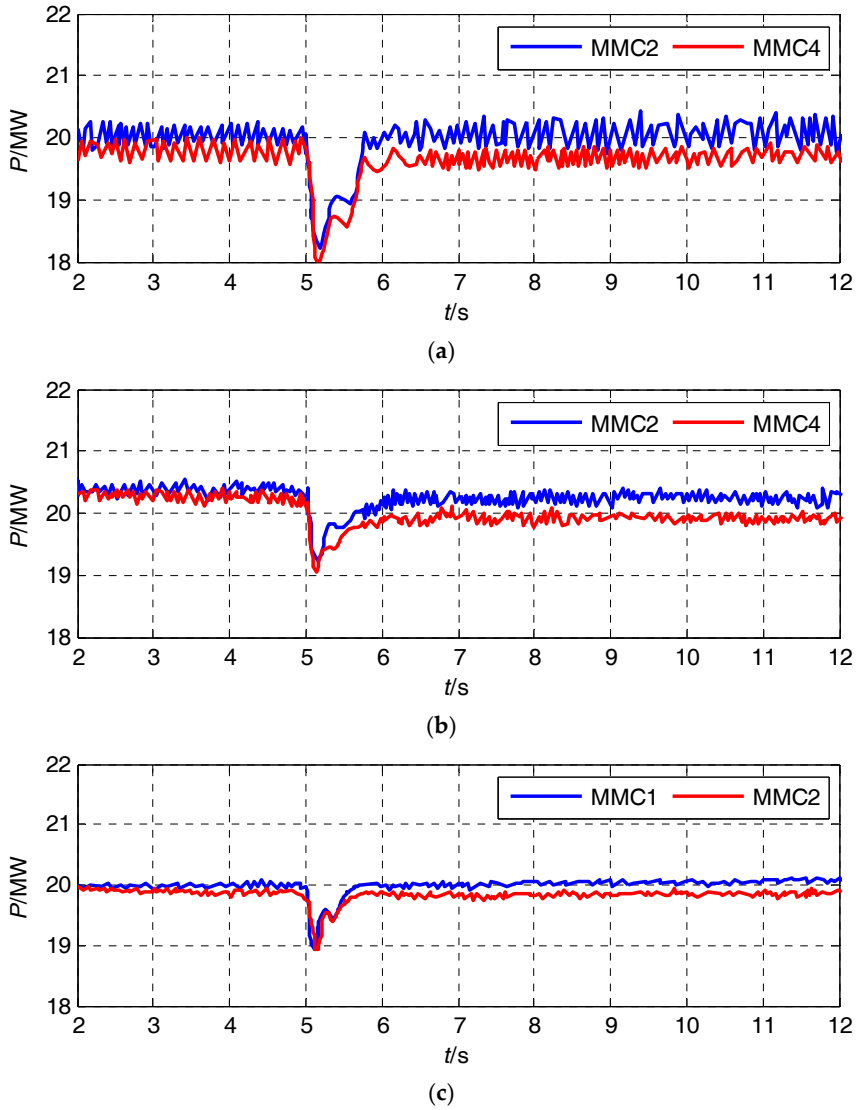

Figure 11. Simulation of the operation during an exit of the input converter station: (**a**) The DC voltage controlled by DCLC; (**b**) the DC voltage controlled by FCS-MPC; (**c**) the DC voltage controlled by HM^2PC.

In this simulation scenario involving a large disturbance where one end completely withdraws from the four-terminal system, all three coordinated controls can still achieve three-terminal power balance. However, the lack of voltage control capability in the master-slave control method causes an overshoot of active power to almost reach the upper limit of the master station control. If the limit is exceeded, it may cause a change in the control master station, thereby forcing the MMC4 station to maintain the DC voltage by reducing the load power. The power adjustment speed of the multi-point voltage control strategy based on an active power balance proposed in this paper performs better than voltage drop control, achieving the minimum voltage fluctuation and power fluctuation in the steady state.

5. The Scheme of Experimental Verification

In order to further verify the effectiveness of the proposed control strategy, a real-time controller hardware-in-the-loop test platform based on RT-LAB (11.1, OPAL-RT technologies Inc, Montreal, QC, Canada) can be built, as shown in Figure 12. The network frame model of MTDC system is built in the upper computer software of RT-LAB. Its main topology is put in the high performance real-time

simulator OP5600 (OPAL-RT technologies Inc, Montreal, QC, Canada) and the high frequency power electronic devices are placed in the nanosecond real-time simulator OP7020 (OPAL-RT technologies Inc., Montreal, QC, Canada) containing FPGA, which are connected to the external controller through the I/O interface and communication protocol. Then, the control strategy proposed in this paper can be rewritten into the form of C language and fed into the external controller (usually Digital Signal Processor (DSP)). In addition, it can test different running scenarios by dynamically adjusting the reference values of state quantities in the control subsystem of OP5600 in real time. In a nutshell, experimental verification is the next research focus that needs to be overcome.

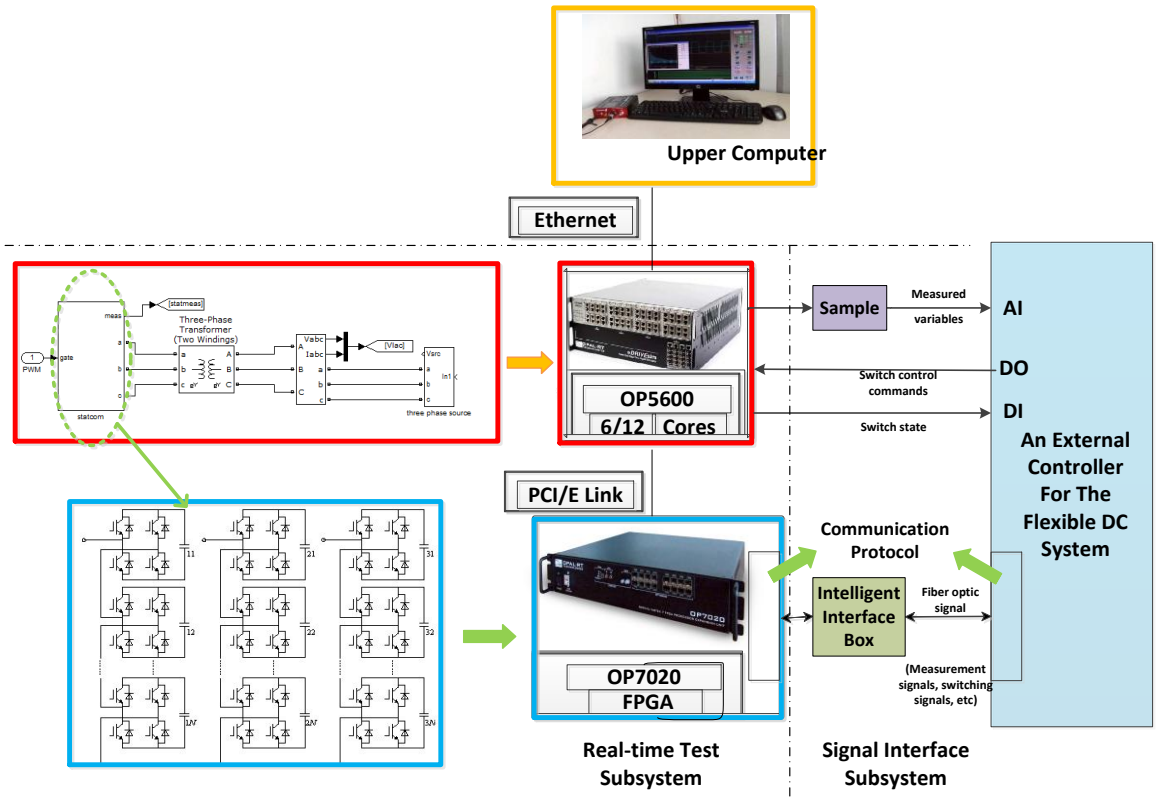

Figure 12. A schematic diagram of the real-time controller hardware-in-the-loop test platform.

6. Conclusions

A hybrid modulated model predictive control (HM^{2}PC) strategy for modular-multilevel-converter (MMC) multi-terminal direct current (MTDC) systems supplying power to passive networks or weak AC systems was developed to improve the control performance of maintaining the DC voltage and power balance of the proposed system. The proposed method, on the basis of fully preserving the superiority of the traditional model predictive control method, reduces the amount of control operations and has the characteristics of flexible structure, good robustness, and strong scalability.

Next, an improved multi-point DC voltage control strategy based on active power balanced control is proposed, which is proved to have a fast transient response and includes the control target directly in the cost function minimization algorithm. It has the further advantage of including a suitable modulation scheme inside the cost function minimization algorithm, in order to maintain a constant switching frequency equal to half the sampling frequency.

Finally, the MMC-MTDC system supplying power to passive networks or weak alternating current systems under different operating conditions is simulated to analyze and demonstrate the feasibility and effectiveness of the proposed control strategy. Besides, the scheme of experimental verification is mentioned in detail.

Author Contributions: All of the authors contributed to this research. The Authors' contributions are as follows: Writing-Original Draft, Z.W.; Writing-Review & Editing, Z.W., J.C. and W.G.; Data Curation and Investigation, Q.H.; Formal Analysis and Supervision, L.C.; Methodology and Resources, X.Y.

Funding: This work was supported by Science and Technology Project of State Grid (J2017037) and The National Natural Science Foundation of China (for youth, 51707033).

Conflicts of Interest: The authors declare no conflict of interest.

References

1. Nami, A.; Liang, J.; Dijkhuizen, F.; Demetriades, G.D. Modular Multilevel Converters for HVDC Applications: Review on Converter Cells and Functionalities. *IEEE Trans. Power Electron.* **2015**, *30*, 18–36. [CrossRef]
2. Ni, Y.X.; Vittal, V.; Kliemann, W.; Fouad, A.A. Nonlinear modal interaction in HVDC/AC power systems with DC power modulation. *IEEE Trans. Power Syst.* **2015**, *11*, 2011–2017. [CrossRef]
3. Li, X.; Song, Q.; Liu, W.; Rao, H.; Xu, S.; Li, L. Protection of Nonpermanent Faults on DC Overhead Lines in MMC-Based HVDC Systems. *IEEE Trans. Power Deliv.* **2013**, *28*, 483–490. [CrossRef]
4. Aleenejad, M.; Mahmoudi, H.; Ahmadi, R. Unbalanced Space Vector Modulation with Fundamental Phase Shift Compensation for Faulty Multilevel Converters. *IEEE Trans. Power Electron.* **2016**, *31*, 7224–7233.
5. Guo, C.; Zhao, C. Supply of an Entirely Passive AC Network through a Double-Infeed HVDC System. *IEEE Trans. Power Electron.* **2010**, *25*, 2835–2841.
6. Lesnicar, A.; Marquardt, R. An innovative modular multilevel converter topology suitable for a wide power range. In Proceedings of the 2003 IEEE Bologna Power Tech Conference Proceedings, Bologna, Italy, 23–26 June 2003; Volume 3, p. 6.
7. Gnanarathna, U.N.; Gole, A.M.; Jayasinghe, R.P. Efficient Modeling of Modular Multilevel HVDC Converters (MMC) on Electromagnetic Transient Simulation Programs. *IEEE Trans. Power Deliv.* **2015**, *26*, 316–324. [CrossRef]
8. Zhang, L.; Harnefors, L.; Nee, H.P. Interconnection of two very weak ac systems by VSC-HVDC links using power-synchronization contro. *IEEE Trans. Power Syst.* **2011**, *26*, 344–355. [CrossRef]
9. Aleenejad, M.; Mahmoudi, H.; Moamaei, P.; Ahmadi, R. A New Fault-Tolerant Strategy Based on a Modified Selective Harmonic Technique for Three-Phase Multilevel Converters with a Single Faulty Cell. *IEEE Trans. Power Electron.* **2016**, *31*, 3141–3150. [CrossRef]
10. Aleenejad, M.; Mahmoudi, H.; Ahmadi, R. A Multi-Fault Tolerance Strategy for Three Phase Cascaded H-Bridge Converters Based on HalfWave Symmetrical Selective Harmonic Elimination Technique. *IEEE Trans. Power Electron.* **2016**, *32*, 7980–7989. [CrossRef]
11. Zhang, L.; Harnefors, L.; Nee, H.P. Modeling and Control of VSC-HVDC Links Connected to Island Systems. *IEEE Trans. Power Syst.* **2011**, *26*, 783–793. [CrossRef]
12. Wang, L. *Model Predictive Control System Design and Implementation Using MATLAB*; Springer Science & Business Media: London, UK, 2009.
13. Yu, F.; Lin, W.; Wang, X.; Xie, D. Fast Voltage-Balancing Control and Fast Numerical Simulation Model for the Modular Multilevel Converter. *IEEE Trans. Power Deliv.* **2015**, *30*, 220–228. [CrossRef]
14. Saad, H.; Guillaud, X.; Mahseredjian, J.; Dennetière, S.; Nguefeu, S. MMC Capacitor Voltage Decoupling and Balancing Controls. *IEEE Trans. Power Deliv.* **2015**, *30*, 704–712. [CrossRef]
15. Moon, J.W.; Kim, C.S.; Park, J.W.; Kang, D.W.; Kim, J.M. Circulating Current Control in MMC Under the Unbalanced Voltage. *IEEE Trans. Power Deliv.* **2013**, *28*, 1952–1959. [CrossRef]
16. Rodriguez, J.; Cortes, P. *Predictive Control of Power Converters and Electrical Drives*; John Wiley & Sons: Hoboken, NJ, USA, 2012.
17. Preindl, M.; Bolognani, S. Optimal State Reference Computation with Constrained MTPA Criterion for PM Motor Drives. *IEEE Trans. Power Electron.* **2015**, *30*, 4524–4535. [CrossRef]
18. Akter, M.P.; Mekhilef, S.; Tan, N.M.; Akagi, H. Model Predictive Control of Bidirectional AC-DC Converter for Energy Storage System. *J. Electr. Eng. Technol.* **2015**, *10*, 165–175. [CrossRef]
19. Narimani, M.; Wu, B.; Yaramasu, V.; Cheng, Z.; Zargari, N.R. Finite Control-Set Model Predictive Control (FCS-MPC) of Nested Neutral Point-Clamped (NNPC) Converter. *IEEE Trans. Power Electron.* **2015**, *30*, 7262–7269. [CrossRef]

20. Kouro, S.; Cortés, P.; Vargas, R.; Ammann, U.; Rodríguez, J. Model Predictive Control-A Simple and Powerful Method to Control Power Converters. *IEEE Trans. Ind. Electron.* **2009**, *56*, 1826–1838. [CrossRef]
21. Geyer, T.; Papafotiou, G.; Morari, M. Model Predictive Direct Torque Control-PartI: Concept, Algorithm, and Analysis. *IEEE Trans. Ind. Electron.* **2009**, *56*, 1894–1905. [CrossRef]
22. Papafotiou, G.; Kley, J.; Papadopoulos, K.G.; Bohren, P.; Morari, M. Model Predictive Direct Torque Control—Part II: Implementation and Experimental Evaluation. *IEEE Trans. Ind. Electron.* **2009**, *56*, 1906–1915. [CrossRef]
23. Cortés, P.; Ortiz, G.; Yuz, J.I.; Rodríguez, J.; Vazquez, S.; Franquelo, L.G. Model Predictive Control of an Inverter With Output, Filter for UPS Applications. *IEEE Trans. Ind. Electron.* **2009**, *56*, 1875–1883. [CrossRef]
24. Qin, J.; Saeedifard, M. Predictive Control of a Modular Multilevel Converter for a Back-to-Back HVDC System. *IEEE Trans. Power Deliv.* **2012**, *27*, 1538–1547.
25. Mariethoz, S.; Fuchs, A.; Morari, M. A VSC-HVDC Decentralized Model Predictive Control Scheme for Fast Power Tracking. *IEEE Trans. Power Deliv.* **2014**, *29*, 462–471. [CrossRef]
26. Preindl, M.; Schaltz, E.; Thogersen, P. Switching Frequency Reduction Using Model Predictive Direct Current Control for High-Power Voltage Source Inverters. *IEEE Trans. Ind. Electron.* **2011**, *58*, 2826–2835. [CrossRef]
27. Xia, C.; Liu, T.; Shi, T.; Song, Z. A Simplified Finite-Control-Set Model-Predictive Control for Power Converters. *IEEE Trans. Ind. Inform.* **2014**, *10*, 991–1002.
28. Zhang, Y.; Tai, N.; Xu, B. Fault Analysis and Traveling-Wave Protection Scheme for Bipolar HVDC Lines. *IEEE Trans. Power Deliv.* **2012**, *27*, 1583–1591. [CrossRef]
29. Rashwan, A.; Sayed, M.A.; Mobarak, Y.; Shabib, G.; Senjyu, T. Predictive Controller Based on Switching State Grouping for a Modular Multilevel Converter with Reduced Computational Time. *IEEE Trans. Power Deliv.* **2017**, *32*, 2189–2198. [CrossRef]
30. Bathurst, G.N.; Watson, N.R.; Arrillaga, J. Modeling of bipolar HVDC links in the harmonic domain. *IEEE Trans. Power Deliv.* **2002**, *15*, 1034–1038.
31. Ilves, K.; Harnefors, L.; Norrga, S.; Nee, H.P. Predictive Sorting Algorithm for Modular Multilevel Converters Minimizing the Spread in the Submodule Capacitor Voltages. *IEEE Trans. Power Electron.* **2015**, *30*, 440–449. [CrossRef]
32. Mahmoudi, H.; Aleenejad, M.; Ahmadi, R. A New Multiobjective Modulated Model Predictive Control Method with Adaptive Objective Prioritization. *IEEE Trans. Ind. Appl.* **2017**, *53*, 1188–1199. [CrossRef]